Direct Electrical Measurements of Energy Bands in Organic Semiconductors by Device-Based Ballistic Carrier Emission Spectroscopy

Hyuk-Jae Jang[1,2,3,], Oleg A. Kirillov[2], John S. Suehle[2], and Curt A. Richter[2]*

[1.] Theiss Research, La Jolla, CA 92037, USA.

[2.] Nanoscale Device Characterization Division, National Institute of Standards and Technology, 100 Bureau Drive, Gaithersburg, MD 20899, USA.

[3.] Western Digital Corporation, 5601 Great Oaks Parkway, San Jose, CA 95119, USA.

ABSTRACT: Understanding the electronic structure of organic/molecular semiconductors and the energetics at their interfaces with metals is critical for organic-based electronics applications. Here we demonstrate that the energetics at metal/molecule interfaces can be electrically measured by ballistic charge carrier (both electron and hole) emission spectroscopy with a single three-terminal device in real operation, thus providing us with direct information on the electronic structures of molecular semiconductors such as their energy bandgap. The energy distribution of electronic states in the molecular semiconductors tailing into their energy bandgap is well described by Lorentzian function in our measurements. In spin-polarized carrier injection measurements, we observe little or no magnetoresistance signal in our magnetic tunnel transistors which indicates that spin filtering effects strongly subside either at the metal/molecule interfaces or in the organic layers.

1. INTRODUCTION

Organic semiconductors and electronically functional molecular materials are being studied intensively for a variety of device applications.[1-2] The injection and extraction of charge carriers in organic-based devices are achieved by a metallic electrode in contact with organic molecules in most cases, and the performance and efficiency of organic-based electronic, optoelectronic, and spintronic devices are critically influenced by the energetics of these metal/molecule interfaces.[3-4] Appropriate experimental information remains critical for accurately modeling and predicting the electronic properties at the metal/organic interfaces and the bandgap in the organic semiconductors in order to fully utilizing the potential of various organic-based devices from optoelectronic to

electronic device applications.[4] In general, information on band energetics at metal/molecule interfaces has been experimentally obtained by measuring the ionization energy (IE) and the electron affinity (EA), which are the energy separation of the highest occupied molecular orbital (HOMO) and the lowest unoccupied molecular orbital (LUMO) from the vacuum level (VL), respectively.[4] For the measurement of the IE, ultraviolet photoemission spectroscopy (UPS) and photoemission yield spectroscopy (PEYS) are commonly used.[3-6] The value of EA is usually estimated by optical bandgap measurements in combination with the measured IE value; however, it can be significantly different from the electronic bandgap in organic molecular systems due to their high excitonic binding energy or the Coulombic stabilization energy of electron-hole pairs.[6] The EA can be determined directly by inverse photoemission spectroscopy (IPES). Unfortunately, the sample often suffers radiation damage or modification during the measurement which can make it difficult to obtain the true value.[4, 7] The Kelvin probe method has been employed to study the energetics of metal/molecule interfaces as well although care is required for physical interpretation of data.[4, 8]

Ballistic electron emission spectroscopy (BEES) is a three-terminal scanning tunneling microscopy (STM)-based technique invented for studying band energetics at the interface of metal-inorganic semiconductor Schottky diodes. BEES provides nanometer spatial resolution owing to the atomic-scale positioning capability of the STM tip.[9-10] Recently, the BEES technique has been adopted for investigating the band energetics of metal/organic molecule interfaces.[11-14] For the investigation of large area interfacial band energetics, one does not need to use a STM tip to perform BEES. A real, operating, three-terminal device can be built and used for BEES as described in Figure 1a.[13-14] The BEES technique avoids excitonic effects and any sample damage by radiation and thus it can provide a true electronic bandgap. The BEES device is composed of

three metallic electrodes (emitter, base, and collector), one oxide tunneling barrier, and an organic semiconductor layer as shown in the inset of Figure 1a. When the emitter voltage, V_E (applied between the emitter and the base) creates a potential difference eV_E larger than the energy barrier eV_b between the base and the LUMO of the organic molecule at their base/molecule interface, ballistic electrons tunneling through the oxide barrier are injected into the LUMO of the organic semiconductor. They are then collected in the collector leading to a sharp rise in the collector current, I_C, at $V_E = V_b$.[9-10] BEES-based devices have been successfully utilized for spintronic applications as well.[15-18] It has been experimentally demonstrated that BEES-based three terminal junctions can overcome the impedance mismatch problem during spin-polarized carrier injection[15-16] and also, they can be used as spin-valve transistors[17] and magnetic tunnel transistors[18] for high magnetoresistance (MR) and high field sensitivity applications. To date, investigations of the energetics at the metal/molecule interface by using BEES-based three terminal devices have been carried out on few molecular materials such as Alq_3 and C_{60}.[13-14] A previous study on metal/C_{60} interface showed the BEES spectra were well fitted with a simple analytical model originally proposed by Bell and Kaiser,[9-10] but without a sharp increase at $V_E = V_b$, which was interpreted as arising from broadening of the molecular levels.[14] In contrast, a study of the metal (Al or Fe)/Alq_3 interface observed that the BEES spectra deviated from the Bell and Kaiser analytical model. This deviation was attributed to space charge accumulation due to sub-energy carrier injection by thermally assisted hopping of charge carriers.[13]

The BEES-based technique can also be used for investigating the HOMO as well as the LUMO as suggested by a report on the metal/inorganic semiconductor interface.[19] As pointed out in the prior studies, by reversing V_E, (a positive emitter bias with respect to the base), the creation of a nonequilibrium hole distribution is achieved. When the magnitude of eV_E is larger than that of eV_b,

holes can enter the HOMO ballistically through a few nanometer thick base layer as illustrated in Figure 1b since the attenuation length of a hole through a metal is generally as large as tens of nanometers.[11, 19] This process is called ballistic hole emission spectroscopy (BHES).[11, 19] In principle, with appropriate emitter biases, both BEES and BHES can be realized in one device if the Fermi level (E_F) of the base metal is located between the HOMO and the LUMO of the organic molecule. In this case, both ballistic holes and electrons can enter the organic layer and they are collected in the collector metal.[11, 19-20] It was reported that the deposition of certain organic materials such as carbon, pentacene, and Alq_3 onto Au films can modify the work function of the Au surface to shift its E_F closer to the midgap energy, half way between the HOMO and the LUMO band edge of those organic materials.[21-23] Taking this work function modification into consideration, we set out to perform BEES and BHES measurements of pentacene and Alq_3 deposited onto Au surfaces by using three-terminal devices with the goal of determining whether both the LUMO and the HOMO of the organic semiconductors and their bandgap can be obtained in a single device. In addition, we designed and fabricated devices with magnetic electrodes so that they can work as magnetic tunnel transistors if the spin filtering effect persists across the metal/molecule interface and through the organic layer.

2. EXPERIMENTAL METHODS

2.1. Preparation of devices

Our three-terminal devices were built on a thermally oxidized (300 nm thick SiO_2) silicon substrate by using mechanical shadow masks and thermal evaporation in vacuum deposition systems. First, the emitter electrode consisting of 10 nm thick $Co_{84}Fe_{16}$ and 3 nm thick Al was made through a shadow mask and then, *ex-situ* oxidation was performed under ozone gas and

heating (around 140 °C for 3 min.) to form an aluminum oxide (AlO_X) layer. After the oxidation, the base electrode consisting of 4 nm thick $Ni_{81}Fe_{19}$ and 4 nm thick Au was constructed through another shadow mask. These devices with a top Au layer was transferred to another vacuum chamber for the deposition of organic molecules (they were exposed to the air during transfer). Two different types of devices were fabricated by thermally evaporating two different organic molecules, pentacene and Alq_3, over the entire area of each respective device. The thicknesses of pentacene and Alq_3 were 70 nm and 60 nm, respectively. The thickness of the deposited organic molecules was chosen so that it is thin enough that ballistic charge carriers can transport through the organic layer and reach the collector, but not so thin that electrical short circuits occur due to pinholes. Finally, the collector electrode made of 100 nm thick Al was fabricated through a shadow mask. The shadow mask was placed on to the sample in a glove box under Ar gas without exposure to ambient air in order to avoid any oxidation and minimize contamination of organic molecules. The film thicknesses were monitored during deposition by a calibrated quartz crystal monitor. A schematic cross-sectional view of the device with electrical circuit connections is illustrated in Figure 2a. The emission area (AlO_X tunnel junction) of the fabricated devices was $\approx 10^4$ μm^2 and the collection area was slightly less than 10^4 μm^2.

2.2. Electrical measurements

The electrical and the magnetoresistance (MR) measurements were carried out in a commercial cryogenic probe station system under vacuum pressure of $\approx 7\times10^{-4}$ Pa ($\approx 5\times10^{-6}$ Torr) at 77 K in darkness. For this study, three pentacene-based devices and two Alq_3-based devices were investigated.

3. RESULTS AND DISCUSSION

3.1. Electrical measurements of ballistic electron and hole injection

Figure 2b displays the emitter current I_E between the emitter and the base electrodes of a pentacene-based device as a function of the emitter bias V_E and Figure 2c shows the collector current I_C between the base and the collector electrodes of the same device as a function of the V_E. As one can see in Figure 2c, we were able to inject both ballistic holes and electrons into the organic layer and collect them at the collector by using the emitter tunnel junction. All the devices had consistently similar tunneling current (the magnitude of I_E was around 2 mA at V_E = 1.5 V), but there was a large variation in the collector current, I_C, from one device to another: the magnitude of I_C ranging from sub-pA to a few tens of nA. Given the large device junction area, the large variation in the magnitude of I_C among devices indicates that the I_C is sensitive to the thickness variation of organic layer. In order to obtain the values of the energy barriers formed at the Au/molecule interface for holes and electrons, we adopted an analytical model proposed by Bell and Kaiser[9-10] and we fitted our experimental data to the model, which is described as a red line in Figure 2c. The theoretical analysis was first carried out by fitting the emitter tunneling current data (I_E *versus* V_E) to the following equation based on Simmons' model with a square tunneling barrier[24]:

$$I_E(V_E) = A \int_0^{E_{max}} D(E_x) \int_0^{\infty} [f(E) - f(E + eV_E)]\, dE_r dE_x, \qquad (1)$$

and

$$D(E_x) \cong e^{\frac{-(E_F + \bar{\varphi} - E_x)^{\frac{1}{2}}}{\lambda}}, \qquad (2)$$

where $A = 4\pi me/h^3$ is a constant, h is the Planck's constant, m is the electron mass, e is the electron charge, $f(E)$ is the Fermi-Dirac distribution, E_x is the energy component of the incident electron in the x direction (see Figure 1 for illustration), E_r is the energy component of the incident

electron in polar coordinates, $\bar{\varphi} = (\varphi - eV_E/2)$ is the mean oxide barrier height, φ is the height of rectangular barrier, E_F is the Fermi level of the emitter, $D(E_x)$ is the transmission probability for an electron (or a hole) to tunnel through the oxide barrier, $E_{max} = E_F + \varphi - eV_{max}$, V_{max} is the maximum value of V_E applied during the experiment, and λ is a constant related to the barrier thickness. For the fitting, $A = 1.61\times10^6$ A/(eV)^2, and $E_F = 4.25$ eV for aluminum[25] are used. After $I_E(V_E)$ curve fitting to the Simmons' model, the values of φ and λ were obtained, and then they are used for fitting the measured collector current curve $I_C(V_E)$ to the Bell and Kaiser model, as described below:

$$I_C(V_E) = R \cdot A \int_0^{E_{max}} D(E_x) \int_0^{\infty} [f(E) - f(E + eV_E)] \cdot \theta(E_x - (E_F - eV_E + eV_b))\, dE_r dE_x \quad (3)$$

where $\theta(E)$ is the Heaviside step function, R is a constant describing a measure of attenuation at the base as well as the organic layer, and eV_b is the energy barrier at the Au/molecule interface as illustrated in Figure 1. Values of φ obtained from fitting $I_E(V_E)$ to Equation (1) range from ≈1.4 eV to ≈2.4 eV for hole injection and from ≈2.2 eV to ≈3.2 eV for electron injection.[26] The average fitting values of eV_b from Equation (3) were 1.56 ± 0.08 eV for electron injection and 1.34 ± 0.08 eV for hole injection at the Au/pentacene interface, and 1.66 ± 0.01 eV for electron injection and 1.40 ± 0.06 eV for hole injection at the Au/Alq_3 interface as illustrated in the insets of Figure 2c. (Described uncertainties are the standard deviations of the mean of fitting values.) Thus, the bandgaps obtained from the Bell and Kaiser model were ≈2.90 eV for pentacene and ≈3.05 eV for Alq_3, respectively. These values are greater than optically measured bandgap values (for example, 2.35 eV for pentacene and 2.7 eV for Alq_3), but smaller than some of suggested electronic (or

transport) bandgaps (for example, 4.1 eV and 4.8 eV for Alq_3).[13, 27-28] As mentioned earlier, the deposition of certain π-conjugated molecules such as carbon, pentacene, and Alq_3 onto Au films can modify the work function of the Au surface to shift its E_F closer to around 4.5 eV.[21-23] If we take this into account, the LUMO and the HOMO of pentacene are ≈2.94 eV and ≈5.84 eV, respectively and the LUMO and the HOMO of Alq_3 are ≈2.85 eV and ≈5.90 eV, respectively.

Figure 3 illustrates the dependence of the I_C (V_E) on the V_C. When a positive (negative) V_C is applied, the applied electric field in the organic layer drives more electrons (holes) to the collector; thus I_C increases. Since the organic layer is highly resistive electrically, this increase in I_C cannot be attributed to the direct current increase in V_C; thus, the base-organic-collector junction exhibits a Schottky diode-like current rectifying behavior (Figure 3b). In addition, one can note that the V_E – I_E characteristics were not affected by the change in the V_C as displayed in Figure 3c. The inset of Figure 3a shows the data of the normalized I_C *versus* V_E with different values of V_C. We observed that as the magnitude of V_C increased, there appeared to be a slight shift in the V_b towards lower values in the I_C(V_E) curve and the curve fitting to the Bell and Kaiser model confirmed that a slight decrease in V_b occurred as the magnitude of the V_C became larger. This decrease in V_b with increasing V_C takes place since an applied bias voltage can lower the barrier height at the Au/organic layer interface as previously reported.[29]

3.2. Analytical approach for band energetics

As can be noticed in Figure 2c, the Bell and Kaiser model did not provide a good fit to the data in the region near $V_E = V_b$. This lower quality fit occurs because the original Bell and Kaiser model is based on the Heaviside step function and assumes an ideally sharp Schottky barrier at the metal/semiconductor interface with a well-defined energy band of the semiconductor.[10] In metal/molecule interfaces, it has been noted that molecular energy bands are broadened, and

available molecular states tail into the molecular bandgap below the LUMO as well as above the HOMO as illustrated in Figure 4a.[14, 30] Particularly for pentacene, it is known that the broadening of molecular energy bands can occur due to microscopic changes during film preparation such as structural inhomogeneity.[31] This discrepancy between the model and the experimental data was also observed in a previous study and in order to accommodate the discrepancy, the Heaviside step function in the Bell and Kaiser model was replaced with a Gaussian distribution function describing the broadening of the density of states in the molecular layer,[14] but this replacement did not work well for fitting the model to our experimental data. In fact, it was previously suggested that the electronic states of π-conjugated molecules in contact with metal substrates are broadened into a Lorentzian function because there is a resonance of the molecular states with the metal continuum of states when the molecules adsorb on the metal surface.[30] Thus, we replaced the step function in the Bell and Kaiser equation with a half Lorentzian distribution function and our modified model provided an excellent fit to the experimental data as shown in Figure 4b and 4c. The Lorentzian distribution function which replaces the Heaviside step function, $\theta(E)$, in Equation (3) and is used for data fitting is described below.

$$\begin{cases} \dfrac{\sigma}{2\pi\cdot\left(\left(\frac{\sigma}{2}\right)^2+\left(E_x-(E_F-eV_E+eV_b)\right)^2\right)} & when\ E_x < (E_F - eV_E + eV_b) \\ 1 & when\ E_x > (E_F - eV_E + eV_b) \end{cases} \quad (4)$$

where σ is full width at half maximum. This modified model extracted larger values of eV_b from the experimental data for both electrons and holes in both pentacene and Alq_3 relative to the ones calculated by the Bell and Kaiser model fitting. This trend suggests that the true electronic bandgaps of both pentacene and Alq_3 are slightly wider than the ones obtained previously. For example, fittings carried out in Figure 4b and 4c produced the values of eV_b for electrons equal to

1.65 eV and those for holes equal to 1.43 eV with the step function. But, when the Equation (4) was adopted into the model, the values of eV_b for electrons and holes became 1.80 eV (with σ = 0.01 eV) and 1.49 eV (with σ = 0.004 eV), respectively. The fitting values obtained from the modified model based on Equation (4) showed larger variation between samples than those from the Bell and Kaiser model thus producing average values with larger uncertainties. This suggests that the degree of hybridization in the electronic states of π-conjugated molecules with Au is different from sample to sample thus resulting in quite different degree of roundedness (or sharpness of I_C rise) near $V_E = V_b$ in V_E - I_C curves. The average fitting values of eV_b from Equation (4) were 1.67 ± 0.12 eV for electron injection and 1.40 ± 0.08 eV for hole injection at the Au/pentacene interface, and 1.99 ± 0.44 eV for electron injection and 2.47 ± 0.62 eV for hole injection at the Au/Alq_3 interface. (Described uncertainties are the standard deviations of the mean of fitting values.)

3.3. Spin-dependent measurements

In addition to determining the band offsets and band gaps at the metal/organic interface, we also tested whether the spin-valve effect[2, 16-18, 32] can be detected in I_C when an in-plane magnetic field was applied to our devices. Since the emitter and the base in our devices each contain a ferromagnetic layer ($Co_{84}Fe_{16}$ for the emitter and $Ni_{81}Fe_{19}$ for the base) as one can see in Figure 2a, our devices are similar to inorganic semiconductor based magnetic tunnel transistors (MTTs).[18, 33] When a V_E is applied between the emitter and the base, spin-polarized ballistic electrons (holes) are injected into the states above (below) E_F of the ferromagnetic base layer by a tunneling process across the AlO_X barrier. After spin-dependent transmission through the ferromagnetic base layer, electrons (holes) can be injected into the LUMO (HOMO) of the organic semiconductor (pentacene and Alq_3 for our study) when the eV_E is greater than the energy barrier

eV_b. The electrons (holes) which transport through the organic layer are collected in the collector. If the magnetic coercivities of the emitter and base electrodes are different, one can detect the spin-valve effect, or tunneling magnetoresistance in I_E when an in-plane external magnetic field is swept. This confirms that spin polarization at the emitter and spin filtering at the base (near E_F) occur. This spin-valve effect can be detected in I_C as well because the spin filtering at the base layer can also occur in ballistic carrier regime above (below) E_F. Previous studies on three terminal MTTs made of inorganic semiconductors showed that the attenuation length of ballistic electrons (holes) with majority spin is much longer than that of those with minority spin when ballistic electrons (holes) are injected into the empty states above (below) the E_F of ferromagnetic thin films, thus providing highly efficient spin filtering effect with large spin valve effect in the I_C.[15-18, 33] For our organic-based devices, we were able to measure the spin-valve effect in I_E as shown in Figure 5a. However, the spin-valve effect is either not present in I_C or exceptionally hard to detect in I_C above ≈1% noise level as shown in Figure 5b. Therefore, based on the very small or no magnetoresistance signal observed in I_C of our three terminal devices made of organic semiconductors, we conclude that the spin filtering effect is drastically diminished either at the metal/molecule interfaces or in the bulk of the organic layer.

4. CONCLUSIONS

In summary, we have experimentally investigated the metal/organic-semiconductor interfacial energetics of Au/pentacene and Au/Alq_3 by using ballistic charge carrier (both electron and hole) emission spectroscopy. We demonstrated that this measurement technique, which allows one to estimate or measure the LUMO and the HOMO of an organic semiconductor simultaneously, can be achieved in a single electronic device simply by reversing the bias and also, it enables a large area measurement with a fully built device, which is useful for understanding band energetics of

other fully built organic-based devices. Our experimental data are fit well by an analytical model which enabled us to determine the *in-situ* interface energy band-offsets and the energy bandgaps of pentacene and Alq_3 films on Au surfaces. These results suggest that energy level broadening at the metal/molecule interface gives rise to a Lorentzian function description due to hybridization of the electronic states of π-conjugated molecules in contact with Au. By using ferromagnetic electrodes to extend the BEES approach into the spin polarized carrier injection regime, we carried out magnetic tunnel transistor measurements which imply that spin filtering effect can be greatly reduced either at the investigated metal/molecule interfaces or in the bulk of the organic layers.

AUTHOR INFORMATION

Corresponding Author

* h.jang@theissresearch.org

ACKNOWLEDGMENT

The authors would like to acknowledge Mr. Anthony Guo for assistance with the experimental set-ups, Ms. Vasileia Georgiou for assistance with device fabrication, Dr. Qin Zhang for assistance with the theoretical analysis. Device fabrication was done in part at the NIST Center for Nanoscale Science and Technology. This work was performed in part under the financial assistance award 70NANB15H303 from the U.S. Department of Commerce, National Institute of Standards and Technology. Certain commercial equipment, instruments, or materials are identified in this paper

in order to specify the experimental procedure adequately. Such identification is not intended to imply recommendation or endorsement by the National Institute of Standards and Technology, nor is it intended to imply that the materials or equipment identified are necessarily the best available for the purpose.

Notes

After the publication of our article, we were contacted by two of our readers regarding a few recent publications,(34−37) which we were not aware of, but are closely related to the work described in our article. After reading those previous publications, we found that those publications would be beneficial to the readers in conjunction with our article. In those four previous publications,(34−37) three-terminal ballistic carrier injection devices were explored theoretically as well as experimentally to study charge as well as spin carrier injection into solution-processed organic semiconductors,(34) C_{60}, and C_{70}(35−37) from a metal layer, and also to investigate their band energetics and charge/spin carrier transport. Those previous reports strongly support the fact that the technique described in our article can be used for a broad range of molecular materials, not limited to the materials investigated in our work, to explore the band energetics and charge/spin carrier injection/transport in molecular-based devices and it delivers valuable and enlightening information to understand characteristics of those devices.

REFERENCES

(1) Editorial, Why Going Organic is Good. *Nat. Mater.* **2009**, *8*, 691.

(2) Jang, H.-J.; Richter, C. A., Organic Spin-Valves and Beyond: Spin Injection and Transport in Organic Semiconductors and the Effect of Interfacial Engineering. *Adv. Mater.* **2017**, *29*, 1602739-1602756.

(3) Jang, H.-J.; Lee, J.-S.; Pookpanratana, S. J.; Hacker, C. A.; Tran, I. C.; Richter, C. A., Modifying Spin Injection Characteristics in the Co/Alq3 System by Using a Molecular Self-Assembled Monolayer. *J. Phys. Chem. C* **2015**, *119*, 12949-12955.

(4) Ishii, H.; Sugiyama, K.; Ito, E.; Seki, K., Energy Level Alignment and Interfacial Electronic Structures at Organic/Metal and Organic/Organic Interfaces. *Adv. Mater.* **1999**, *11*, 605-625.

(5) Gutmann, F.; Lyons, L. E., *Organic Semiconductors*; Wiely: New York, 1967.

(6) Scott, J. C. Metal–Organic Interface and Charge Injection in Organic Electronic Devices. *J. Vac. Sci. Technol., A* **2003**, *21*, 521-531.

(7) Hill, I. G.; Kahn, A.; Soos, Z. G.; Pascal, J. R. A. Charge-Separation Energy in Films of π-Conjugated Organic Molecules. *Chem. Phys. Lett.* **2000**, *327*, 181-188.

(8) Pfeiffer, M.; Leo, K.; Karl, N. Fermi Level Determination in Organic Thin Films by the Kelvin Probe Method. *J. Appl. Phys.* **1996**, *80*, 6880-6883.

(9) Bell, L. D.; Kaiser, W. J. Observation of Interface Band Structure by Ballistic-Electron-Emission Microscopy. *Phys. Rev. Lett.* **1988**, *61*, 2368-2371.

(10) Kaiser, W. J.; Bell, L. D. Direct Investigation of Subsurface Interface Electronic Structure by Ballistic-Electron-Emission Microscopy. *Phys. Rev. Lett.* **1988**, *60*, 1406-1409.

(11) Troadec, C.; Kunardi, L.; Chandrasekhar, N. Ballistic Emission Spectroscopy and Imaging of a Buried Metal⁄Organic Interface. *Appl. Phys. Lett.* **2005**, *86*, 072101-072103.

(12) Li, W.; Kavanagh, K. L.; Matzke, C. M.; Talin, A. A.; Léonard, F.; Faleev, S.; Hsu, J. W. P. Ballistic Electron Emission Microscopy Studies of Au/Molecule/n-GaAs Diodes. *The J. Phys. Chem. B* **2005**, *109*, 6252-6256.

(13) Jiang, J. S.; Pearson, J. E.; Bader, S. D. Direct Determination of Energy Level Alignment and Charge Transport at Metal-Alq3 Interfaces via Ballistic-Electron-Emission Spectroscopy. *Phys. Rev. Lett.* **2011**, *106*, 156807-156810.

(14) Gobbi, M.; Pietrobon, L.; Atxabal, A.; Bedoya-Pinto, A.; Sun, X.; Golmar, F.; Llopis, R.; Casanova, F.; Hueso, L. E. Determination of Energy Level Alignment at Metal/Molecule Interfaces by in-Device Electrical Spectroscopy. *Nat. Commun.* **2014**, *5*, 4161-4167.

(15) Appelbaum, I.; Huang, B.; Monsma, D. J. Electronic Measurement and Control of Spin Transport in Silicon. *Nature* **2007**, *447*, 295-298.

(16) Jang, H.-J.; Appelbaum, I. Spin Polarized Electron Transport near the Si/SiO_2 Interface. *Phys. Rev. Lett.* **2009**, *103*, 117202-117205.

(17) Monsma, D. J.; Vlutters, R.; Shimatsu, T.; Keim, E. G.; Mollema, R. H.; Lodder, J. C. Development of the Spin-Valve Transistor. *IEEE Trans. Magn.* **1997**, *33*, 3495-3499.

(18) Jiang, X.; van Dijken, S.; Wang, R.; Parkin, S. S. P. Bias Voltage Dependence of Magnetocurrent in Magnetic Tunnel Transistors. *Phys. Rev. B* **2004**, *69*, 014413-014418.

(19) Hecht, M. H.; Bell, L. D.; Kaiser, W. J.; Davis, L. C. Ballistic-Hole Spectroscopy of Interfaces. *Phys. Rev. B* **1990**, *42*, 7663-7666.

(20) Yi, W.; Narayanamurti, V.; Lu, H.; Scarpulla, M. A.; Gossard, A. C.; Huang, Y.; Ryou, J.-H.; Dupuis, R. D. Bandgap and Band Offsets Determination of Semiconductor Heterostructures Using Three-Terminal Ballistic Carrier Spectroscopy. *Appl. Phys. Lett.* **2009**, *95*, 112102-112104.

(21) Kahn, A. Fermi Level, Work Function and Vacuum Level. *Mater. Horiz.* **2016**, *3*, 7-10.

(22) Koch, N.; Kahn, A.; Ghijsen, J.; Pireaux, J.-J.; Schwartz, J.; Johnson, R. L.; Elschner, A. Conjugated Organic Molecules on Metal versus Polymer Electrodes: Demonstration of a Key Energy Level Alignment Mechanism. *Appl. Phys. Lett.* **2003**, *82*, 70-72.

(23) Bröker, B.; Blum, R.-P.; Frisch, J.; Vollmer, A.; Hofmann, O. T.; Rieger, R.; Müllen, K.; Rabe, J. P.; Zojer, E.; Koch, N. Gold Work Function Reduction by 2.2eV with an Air-Stable Molecular Donor Layer. *Appl. Phys. Lett.* **2008**, *93*, 243303-243305.

(24) Simmons, J. G. Generalized Formula For the Electric Tunnel Effect between Similar Electrodes Separated by a Thin Insulating Film. *J. Appl. Phys.* **1963**, *34*, 1793-1803.

(25) Mitchell, E. W. J.; Mitchell, J. W. The Work Functions of Copper, Silver and Aluminium. *Proc. R. Soc. London, Ser. A* **1951**, *210*, 70-84.

(26) Rottländer, P.; Hehn, M.; Schuhl, A. Determining the Interfacial Barrier Height and its Relation to Tunnel Magnetoresistance. *Phys. Rev. B* **2002**, *65*, 054422-054427.

(27) Knupfer, M.; Peisert, H.; Schwieger, T. Band-Gap and Correlation Effects in the Organic Semiconductor Alq3. *Phys. Rev. B* **2001**, *65*, 033204-033207.

(28) Baldacchini, C.; Mariani, C.; Betti, M. G.; Gavioli, L.; Fanetti, M.; Sancrotti, M. Molecular Gap and Energy Level Diagram for Pentacene Adsorbed on Filled d-Band Metal Surfaces. *Appl. Phys. Lett.* **2006**, *89*, 152119-152121.

(29) Rikken, G. L. J. A.; Braun, D.; Staring, E. G. J.; Demandt, R. Schottky Effect at a Metal-Polymer Interface. *Appl. Phys. Lett.* **1994**, *65*, 219-221.

(30) Braun, S.; Salaneck, W. R.; Fahlman, M. Energy-Level Alignment at Organic/Metal and Organic/Organic Interfaces. *Adv. Mater.* **2009**, *21*, 1450-1472.

(31) Yoshida, H.; Yamada, K.; Tsutsumi, J.; Sato, N. Complete Description of Ionization Energy and Electron Affinity in Organic Solids: Determining Contributions from Electronic Polarization, Energy Band Dispersion, and Molecular Orientation, *Phys. Rev. B* **2015**, *92*, 075145-075157.

(32) Jang, H.-J.; Pernstich, K. P.; Gundlach, D. J.; Jurchescu, O. D.; Richter, C. A. Observation of Spin-Polarized Electron Transport in Alq3 by Using a Low Work Function Metal. *Appl. Phys. Lett.* **2012**, *101*, 102412-102416.

(33) Park, B. G.; Banerjee, T.; Lodder, J. C.; Jansen, R. Opposite Spin Asymmetry of Elastic and Inelastic Scattering of Nonequilibrium Holes Injected into a Ferromagnet. *Phys. Rev. Lett.* **2006**, *97*, 137205-137208.

(34) Atxabal, A.; Braun, S.; Arnold, T.; Sun, X.; Parui, S.; Liu, X.; Gozalvez, C.; Llopis, R.; Mateo-Alonso, A.; Casanova, F.; Ortmann, F.; Fahlman, M.; Hueso, L. E. Energy Level Alignment at Metal/Solution-Processed Organic Semiconductor Interfaces.. Adv. Mater. 2017, **29**, 1606901– 1606906, DOI: 10.1002/adma.201606901

(35) Arnold, T.; Atxabal, A.; Parui, S.; Hueso, L. E.; Ortmann, F. Hot Electrons and Hot Spins at Metal–Organic Interfaces. Adv. Funct. Mater. 2018, **28**, 1706105– 170619, DOI: 10.1002/adfm.201706105

(36) Atxabal, A.; Arnold, T.; Parui, S.; Zuccatti, E.; Cinchetti, M.; Casanova, F.; Ortmann, F.; Hueso, L. E. Molecular Spectroscopy in a Solid-State Device. Mater. Horiz. 2019, **6**, 1663–1668, DOI: 10.1039/C9MH00218A

(37) Atxabal, A.; Arnold, T.; Parui, S.; Hutsch, S.; Zuccatti, E.; Llopis, R.; Cinchetti, M.; Casanova, F.; Ortmann, F.; Hueso, L. E. Tuning the Charge Flow between Marcus Regimes in an Organic Thin-Film Device. Nat. Commun. 2019, **10**, 2089– 2095, DOI: 10.1038/s41467-019-10114-2

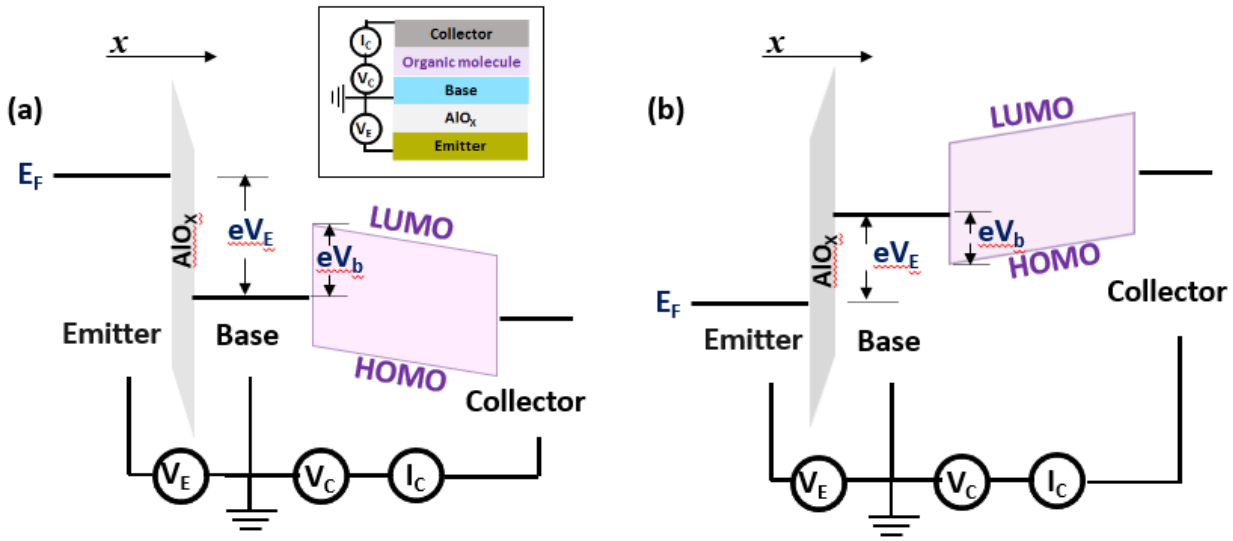

Figure 1. Schematic energy diagrams of a three terminal device performing ballistic (a) electron and (b) hole emission spectroscopy of organic molecules. The sign of the emitter voltage (V_E)

determines either ballistic electron (negative V_E) or hole (positive V_E) injection into the organic layer. This charge carrier injection produces a collector current, I_C, when the magnitude of eV_E is larger than the barrier height eV_b. Application of the collector bias V_C can increase the I_C. Inset: cross-sectional view and electrical connections of generic BEES device structure.

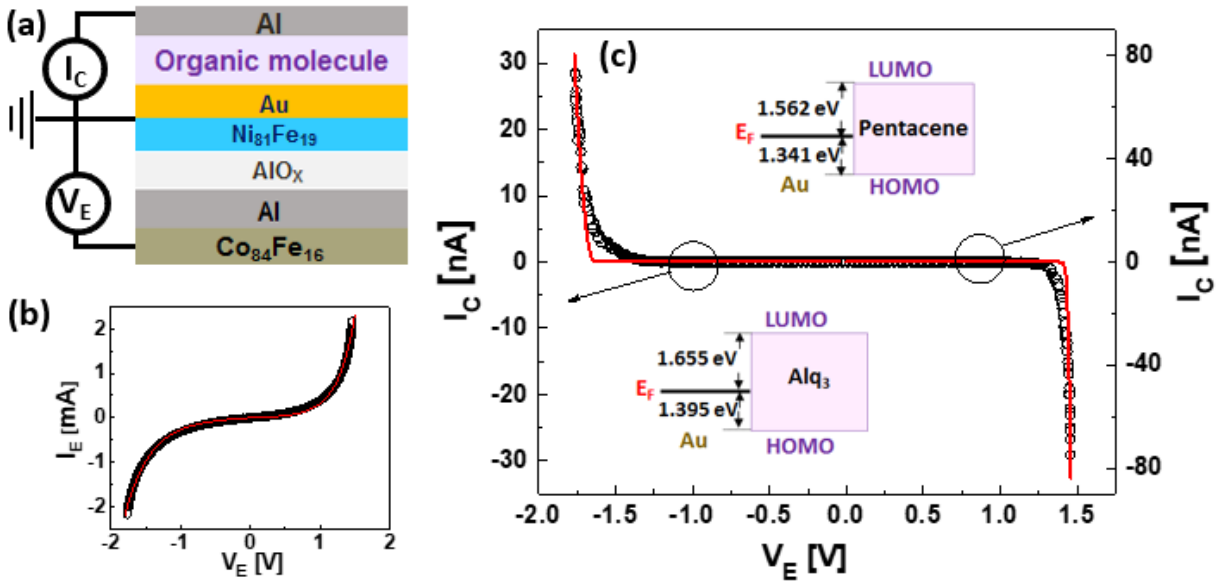

Figure 2. (a) Cross-sectional view and electrical connection of three terminal device. (b) I_E *versus* V_E of pentacene device obtained in experiment (black open circle) and in Simmons model fitting (red line). (c) I_C *versus* V_E of pentacene device obtained in experiment (black open circle) and in Bell and Kaiser model fitting (red line). Please note the different current scales in (b) and (c). Insets: fitting values of barrier heights for electrons and holes of pentacene (top) and Alq_3 (bottom) in contact with Au.

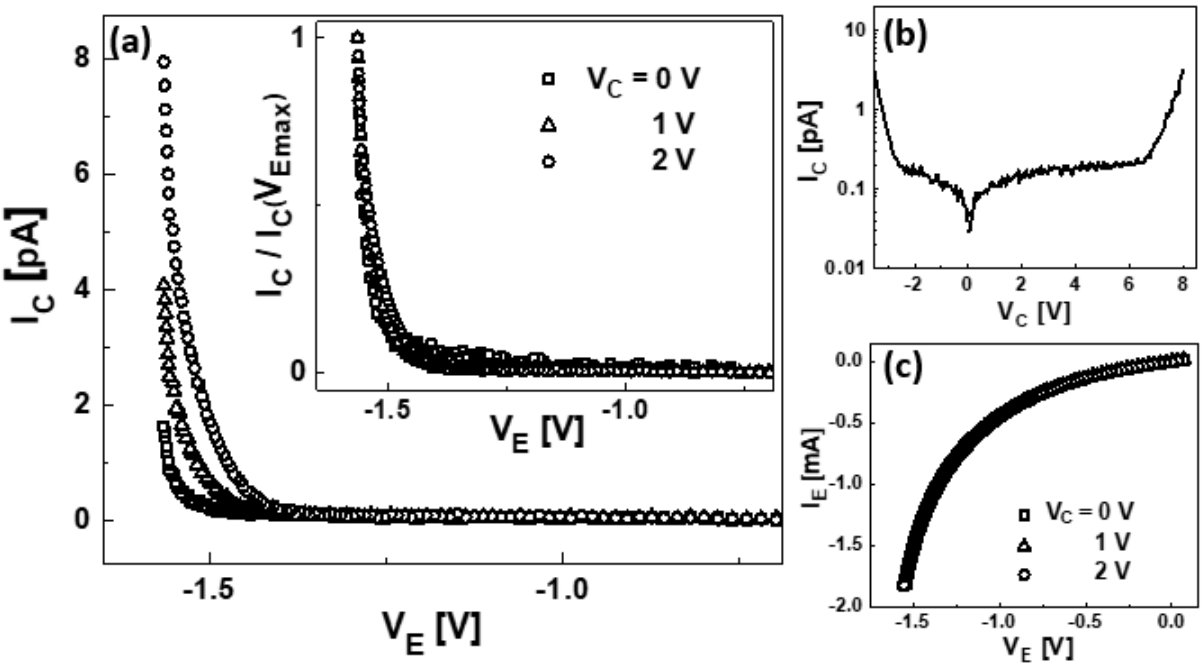

Figure 3. (a) I_C *versus* V_E of pentacene device when V_C = 0 (open square), 1 (open triangle), and 2 V (open circle). Inset: normalized I_C *versus* V_E of three different values of V_C. V_{Emax} was -1.564 V. Obtained values of eV_b for V_C = 0, 1, and 2 V by fitting the data to the model were 1.540, 1.533, and 1.530 eV, respectively. (b) I_C *versus* V_C of pentacene device. (c) I_E *versus* V_E of pentacene device when V_C = 0, 1, and 2 V.

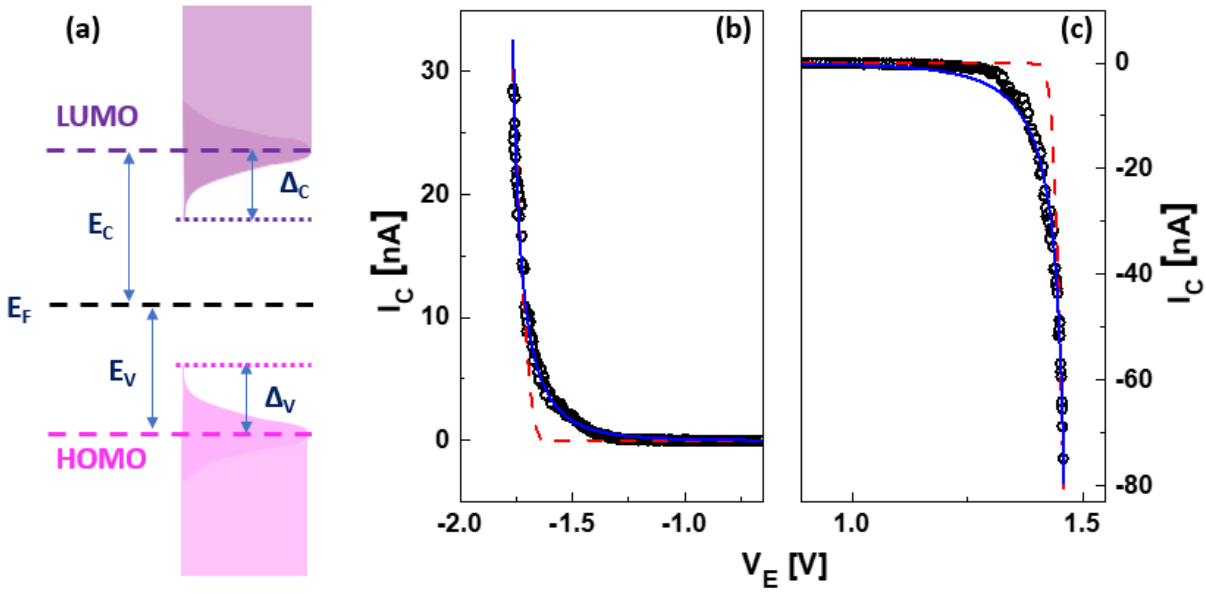

Figure 4. (a) Schematic energy diagram of an organic molecule in contact with a metal describing the broadening of its energy level. E_C and E_V describe the LUMO and the HOMO, respectively. Δ_C and Δ_V illustrate their broadening. *I_C versus V_E* of pentacene device for (b) electron and (c) hole injection measured in experiment (black open circle) and fits to the Bell and Kaiser model with a Heaviside step function (red dashed line) and Lorentzian function (blue solid line).

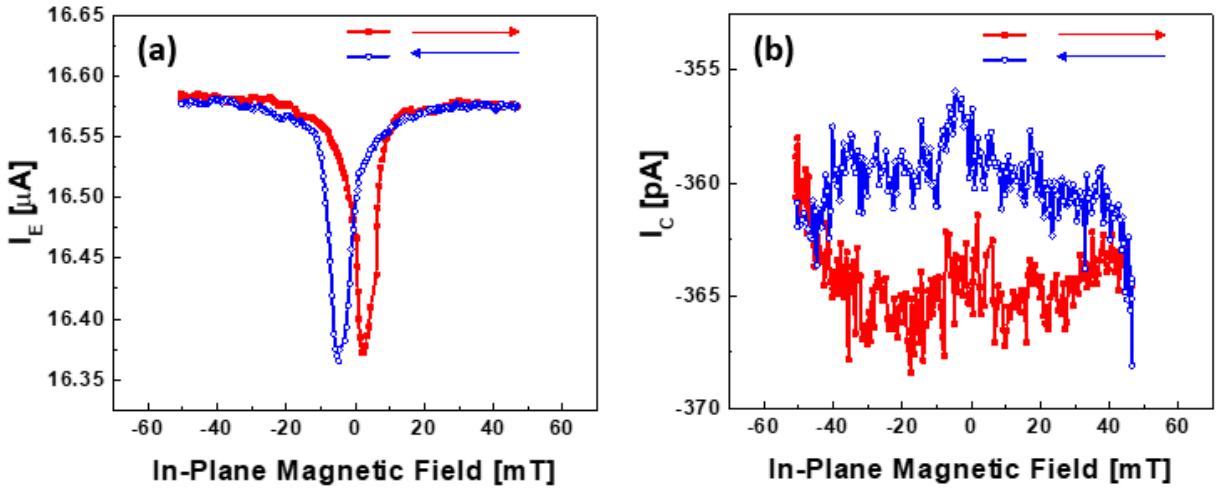

Figure 5. Measured (a) I_E and (b) I_C of pentacene device while sweeping an external magnetic field between -50 mT and 50 mT. Arrows indicate the field sweep direction. During I_E measurement, V_E was 0.1 V. For I_C measurement, V_E and V_C were 3 V and -2.5 V, respectively.

TOC Graphic

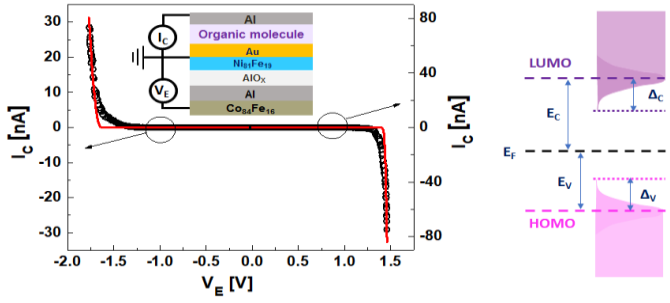
Al
Organic molecule
Au
Ni81Fe19
AlOx
Al
Co84Fe16
IC
VE
IC [nA]
VE [V]
LUMO
HOMO
EC
EF
EV
ΔC
ΔV